Geophysical Journal International

Geophys. J. Int. (2014) **198,** 906–921
GJI Seismology

doi: 10.1093/gji/ggu169

Seismogenic magma intrusion before the 2010 eruption of Eyjafjallajökull volcano, Iceland

J. Tarasewicz,[1] R. S. White,[1] B. Brandsdóttir[2] and C.M. Schoonman[1]

[1] *Bullard Laboratories, Department of Earth Sciences, University of Cambridge, Cambridge, CB3 0EZ, UK. E-mail: jon.tarasewicz@cantab.net*
[2] *Institute of Earth Sciences, Science Institute, University of Iceland, Reykjavík, Iceland*

Accepted 2014 May 6. Received 2014 May 2; in original form 2014 February 24

SUMMARY

We present relatively relocated earthquake hypocentres for >1000 microearthquakes ($M_L < 3$) that occurred during the 2 weeks immediately prior to the 2010 March 20 fissure eruption at Fimmvörðuháls on the flank of Eyjafjallajökull volcano in Iceland. Our hypocentre locations lie predominantly in horizontally separated clusters spread over an area of 10 km^2 and approximately 4 km below sea level (5 km below the surface). Seismic activity in the final 4 d preceding the eruption extended to shallower levels <2 km below sea level and propagated to the surface at the Fimmvörðuháls eruption site on the day the eruption started. We demonstrate using synthetic data that the observed apparent ∼1 km vertical elongation of seismic clusters is predominantly an artefact caused by only small errors (0.01–0.02 s) in arrival time data. Where the signal-to-noise ratio was sufficiently good to make subsample arrival time picks by cross-correlation of both *P*- and *S*-wave arrivals, the mean depth of 103 events in an individual cluster were constrained to 3.84 ± 0.06 km. Epicentral locations are significantly less vulnerable to arrival time errors than are depths for the seismic monitoring network we used. Within clusters of typically 100 recorded earthquakes, most of the arrivals exhibit similar waveforms and identical patterns of *P*-wave first-motion polarities across the entire monitoring network. The clusters of similar events comprise repetitive sources in the same location with the same orientations of failure, probably on the same rupture plane. The epicentral clustering and similarity of source mechanisms suggest that much of the seismicity was generated at approximately static constrictions to magma flow in an inflating sill complex. These constrictions may act as a form of valve in the country rock, which ruptures when the melt pressure exceeds a critical level, then reseals after a pulse of melt has passed through. This would generate recurring similar source mechanisms on the same weak fault plane as the connection between segments of the sill system is repeatedly refractured in the same location. We infer that the magmatic intrusion causing most of the seismicity was likely to be a laterally inflating complex of sills at about 4 km depth, with seismogenic pinch-points occurring between aseismic compartments of the sills, or between adjacent magma lobes as they inflated. During the final 4 d preceding the eruption onset between 22:30 and 23:30 UTC on 2010 March 20, the seismicity suggests that melt progressed upwards to a depth of ∼2 km. This seismicity was probably caused by fracturing of the country rock at the margins of the propagating dyke. Subsequently, on the morning of the eruption a dyke propagated eastward from the region of precursory seismic activity to the Fimmvörðuháls eruption site.

Key words: Fracture and flow; Earthquake source observations; Volcano seismology; Physics of magma and magma bodies; Magma chamber processes; Magma migration and fragmentation.

1 INTRODUCTION

Elevated levels of seismicity under volcanoes have long been interpreted as evidence of magma migration or accumulation in the subsurface. This is frequently corroborated by a subsequent eruption, or by surface deformation consistent with the inflation or deflation of magmatic intrusions. However, relating the observed seismicity to specific, local, magmatic processes is not trivial. The spatial distribution of seismicity can illuminate only the seismogenic parts of the magmatic plumbing system. These are places where the fluid flow or fluid pressure causes locally increased stress that generates failure and volcano-tectonic earthquakes. Subsurface volumes that

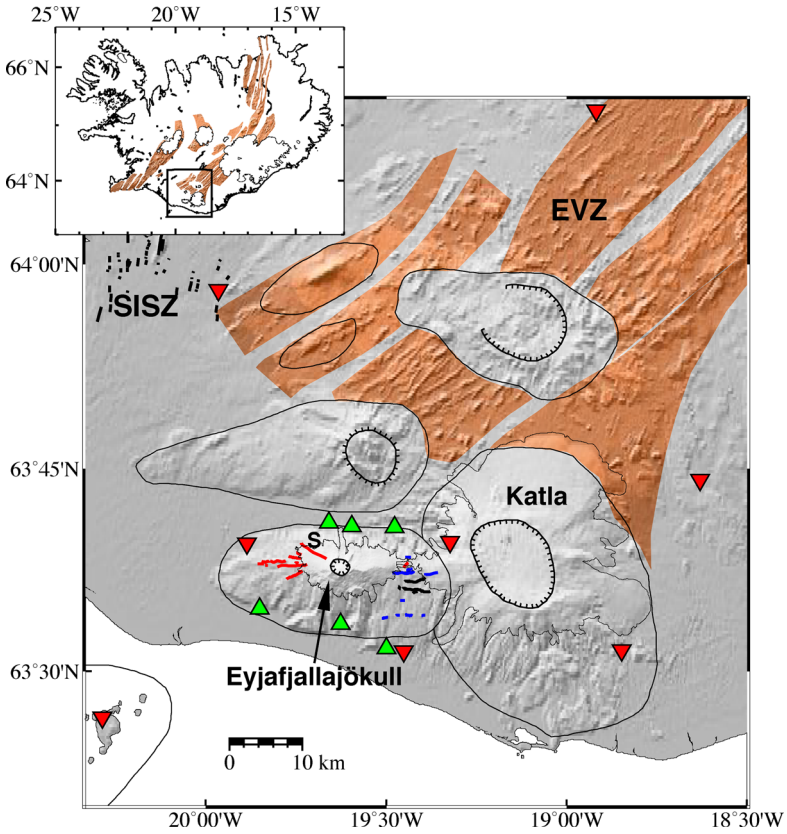

Figure 1. Regional location map and seismic network. Green triangles show temporary seismometers; red triangles show permanent seismometers operated by the Iceland Meteorological Office (IMO). Thin black lines with light grey-scale fill show extent of glacial caps on Eyjafjallajökull and Katla volcanoes. Thicker black outlines show central volcanoes; associated fissure swarms are shaded in brown (Einarsson & Sæmundsson 1987). These volcanic systems form part of the Eastern Volcanic Zone (EVZ). Tick-marked lines show summit craters and calderas. Thick black lines show faults in the South Iceland Seismic Zone (SISZ; Einarsson 2010) and near Eyjafjallajökull. Thick red lines are Holocene eruption fissures; blue lines are older hyaloclastite ridges (www.earthice.hi.is; Jóhannesson & Sæmundsson 1998). 'S' indicates Skerin ridge (Óskarsson 2009). Inset shows map of Iceland with volcanic systems shown in brown, each comprising a central volcano and associated fissure swarm (Einarsson & Sæmundsson 1987); glaciers are shown in white with black outline; black box shows extent of main figure.

exhibit no earthquake activity may represent either solid crust with no melt flowing through it, or regions where melt is migrating, but doing so aseismically through open conduits. We present an analysis of microseismic activity recorded prior to the 2010 eruption of Eyjafjallajökull volcano in Iceland (Fig. 1), which shows that seismicity accompanying the inflation of a broad magmatic intrusion was concentrated in spatially fixed locations.

Eyjafjallajökull volcano is located in the propagating southern part of the Eastern Volcanic Zone (EVZ) in South Iceland (Fig. 1). Northwest of Eyjafjallajökull, the EVZ intersects with the South Iceland Seismic Zone (SISZ), which accommodates overall left-lateral motion along an east–west transform by bookshelf faulting on right-lateral, north–south oriented, strike-slip faults (Einarsson 1991). South of the intersection with the SISZ, the EVZ is characterized by large volcanoes and a lack of conspicuous rift structures. The east–west elongated Eyjafjallajökull volcanic edifice is linked to the larger adjacent Katla volcanic system through east–west striking faults and eruptive fissures (Fig. 1). Eyjafjallajökull volcano has a maximum elevation of 1651 m a.s.l. at a nunatak on the rim of the summit caldera (Larsen *et al.* 2012). The volcano is ice-capped with a maximum ice thickness of ∼200 m (Magnússon *et al.* 2012) before the 2010 eruptions.

Seismic monitoring of Eyjafjallajökull since the early 1970s did not detect any significant number of earthquakes before 1991 (Einarsson & Brandsdóttir 2000; Jakobsdóttir 2008). Many more earthquakes were detected at Eyjafjallajökull during 1992–2000, after which seismic activity dropped and remained low until 2009 (Hjaltadóttir *et al.* 2012).

Intense seismic swarms beneath Eyjafjallajökull in 1994, 1996 and 1999–2000 indicate that intrusive activity occurred beneath the volcano in those years (Hjaltadóttir *et al.* 2009). In 1994 and 1999–2000 magmatic intrusions are inferred to have been emplaced at a depth of 3.5–6.5 km based on surface deformation measurements and seismicity (Dahm & Brandsdóttir 1997; Sturkell *et al.* 2003; Pedersen & Sigmundsson 2004, 2006). Seismicity associated with the 1996 intrusion was predominantly at a much greater depth of 20–25 km, indicating the emplacement of an intrusion near the base of the crust (Hjaltadóttir *et al.* 2009). The 1996 intrusion was too deep to produce a detectable surface deformation signal. In 2009 there was an increase in seismicity after a decade of only subdued activity. A swarm of 200 events was recorded during 2009 June–August, mostly at 9–11 km depth northeast of the summit crater. This was interpreted as indicating a small intrusion in a similar location to the 1999–2000 intrusion (Hjaltadóttir *et al.* 2009).

Seismic activity increased markedly in 2010 January and remained high during February before peaking in early March (Hjaltadóttir *et al.* 2012). Seismic activity remained elevated in 2010 March until reducing in intensity a few days before the eruption began (Tarasewicz *et al.* 2012a).

Geodetic measurements of surface deformation indicate inflation of the east flank of Eyjafjallajökull during 2010 January–March, coinciding with the elevated levels of seismicity (Sigmundsson *et al.* 2010). Particularly high and variable rates of deformation were observed after March 4, before the eruption started on March 20. This latter period, 2010 March 5–20, coincides with the period from which seismic data are presented in this paper. Modelling of the surface deformation during 2010 March suggests the inflation of both a horizontal sill at ∼4–6 km depth under the southeast flank of the volcano and a northwest-dipping dyke that extends from 3–6 km depth up to within a few hundred metres, or less, of the surface. The flow rate into the geodetically modelled intrusions was inferred to be 2–3 m^3s^{-1} in 2010 January–February and 30–40 m^3s^{-1} in 2010 March, with a total estimated pre-eruption intrusion volume in that 3-month period of ∼0.05 km^3 (Sigmundsson *et al.* 2010).

GPS measurements around Eyjafjallajökull show far-field sites moving towards the volcano, indicating deflation of a deep source (>20 km), starting around 2010 February 20 (Hreinsdóttir *et al.* 2012). This suggests that the observed inflation of shallower intrusions was fed by the transport of melt into the mid-crust from a deflating deep source before the onset of the eruption (Gudmundsson *et al.* 2012b). Tapping of deep sills containing melt during the subsequent summit eruption has been postulated from the later seismicity by Tarasewicz *et al.* (2012b).

The eruption began between 22:30 and 23:30 UTC on 2010 March 20 with the extrusion of alkali basalt from a short (<1 km long) fissure on the east flank of the volcano at Fimmvörðuháls, the saddle between the two glaciers that cap the Eyjafjallajökull and Katla volcanoes (Figs 1 and 2). Eruptive activity comprised effusive lava flows with multiple fire fountains along the fissure, reaching up to ∼180 m in height (Höskuldsson *et al.* 2012). A second fissure opened on March 31, slightly to the west and approximately perpendicular to the first. The flank eruption terminated after 3 weeks in the afternoon of 2010 April 12.

A total lava volume of ∼20 × 10^6 m^3 was erupted at Fimmvörðuháls (Edwards *et al.* 2012). However, despite this amounting to ∼40 per cent of the estimated pre-eruption intrusion volume of ∼0.05 km^3, only negligible surface deformation was detected geodetically during the flank eruption (Sigmundsson *et al.* 2010). Geobarometric analyses also indicate that the mafic flank magma had partially crystallized at 16–18 km depth before erupting (Keiding & Sigmarsson 2012). The lack of observed deflation may be explained by the mafic flank magma having a deeper source than the shallow intrusion and either bypassing it or flowing through it but counterbalancing the volume erupted from it with inflow of fresh magma during the eruption (Sigmundsson *et al.* 2010; Gudmundsson *et al.* 2012b).

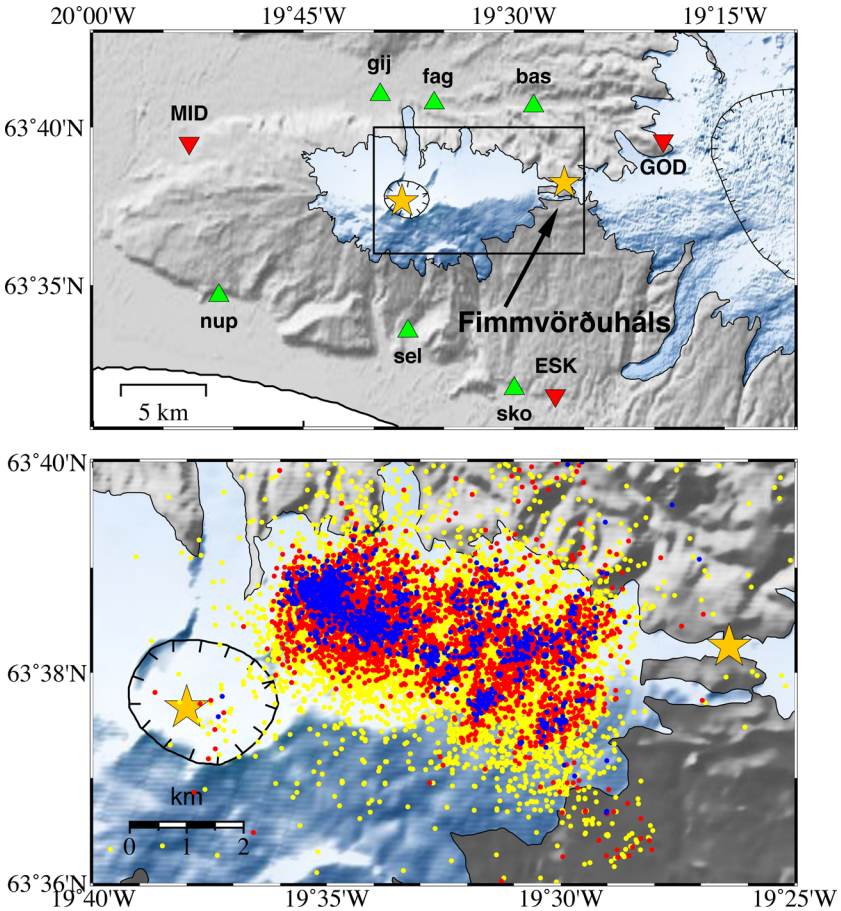

Figure 2. (Top panel) Map showing the closest seismometer locations operating around Eyjafjallajökull during 2010 March 5–20 (triangles, colour-coding as in Fig. 1). Box shows outline of bottom map. (Bottom panel) Map view of >20 000 CMM earthquake locations recorded during 2010 March 5–20 before the Fimmvörðuháls eruption began on 2010 March 20. Events are colour-coded by strength of their coalescence signal in CMM, stated as a signal-to-noise ratio (SNR). Yellow events have 2.0 ≤ SNR ≤ 2.5; red 2.5 < SNR ≤ 3.5; blue SNR > 3.5. Orange stars show location of Fimmvörðuháls fissure eruption on 2010 March 20 (eastern star), and subsequent explosive eruption from the summit crater (western star) that began on 2010 April 14.

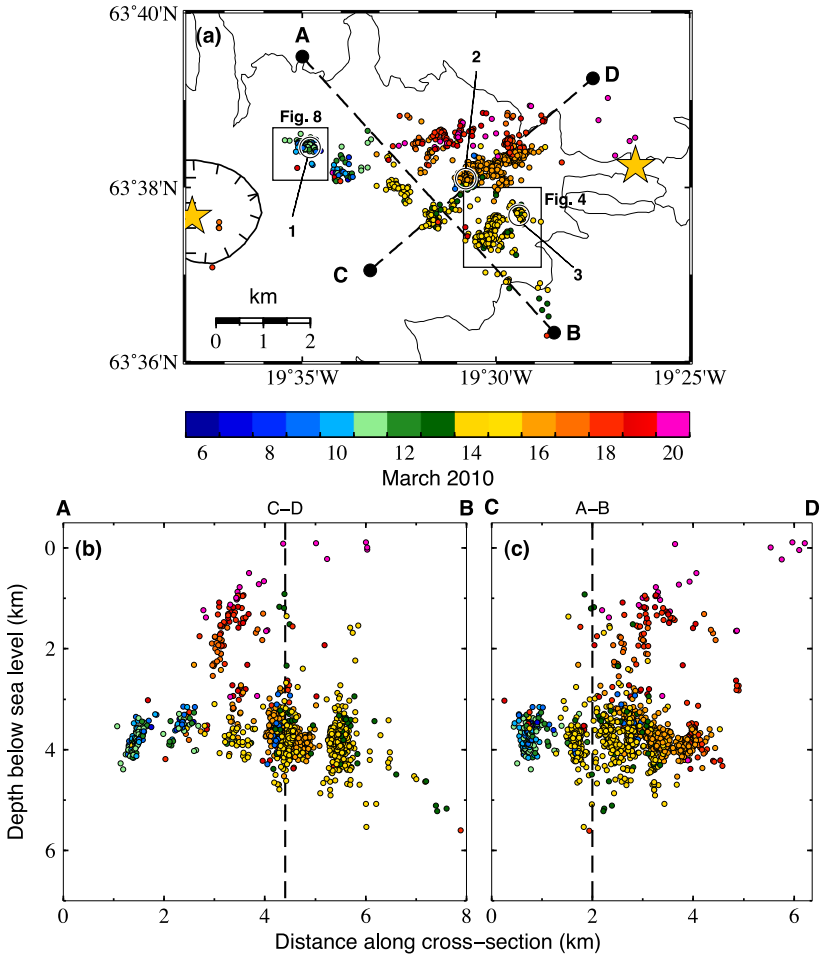

Figure 3. Relatively relocated hypocentres for 1061 events with manually picked arrival times. Event hypocentres are colour-coded by date. Orange stars show Fimmvörðuháls (east) and Eyjafjallajökull summit (west) eruption sites. (a) Map view. (b–c) Cross-sections of hypocentres projected onto lines A–B and C–D, respectively. Boxes mark clusters shown in detail in Figs 4 and 8. Circles labelled 1–3 show locations of fault-plane solutions shown in Fig. 12. See also Animation 1.

Less than 2 d after the flank eruption ended, an eruption from the summit of Eyjafjallajökull began from a subglacial fissure at ∼01:15 UTC on 2010 April 14, 8 km west of the flank eruption site (Gudmundsson *et al.* 2012a,b). A brief subglacial phase was followed by a vigorous explosive phase that evolved into a period of prolonged, continuous, explosive activity that varied in eruption rate and sustained an ash plume 1000–9000 m high. The explosive activity dropped markedly after May 17 and continuous eruption stopped on May 22. Only sporadic minor bursts of activity occurred after this until 17 June, when the eruption terminated (Gudmundsson *et al.* 2012a,b).

The seismicity recorded during the summit eruption extended to depths of over 30 km (Tarasewicz *et al.* 2012a,b). In this paper, we focus on the intense seismicity that preceded both the flank and summit eruptions and is related to the inflation of a shallow intrusion under the flank of the volcano between the two eruption sites.

2 EARTHQUAKE HYPOCENTRE LOCATIONS

2.1 Hypocentre location procedure

We have used seismic data recorded by six Reftek RT130–01 three-component seismometers with Lennartz 5 s sensors that were deployed temporarily to monitor activity at Eyjafjallajökull (Figs 1 and 2). In addition, we have used data from eight stations in the permanent monitoring network operated by the Icelandic Meteorological Office (IMO). All data were recorded at 100 samples per second (sps) with GPS timing.

Hypocentre locations were obtained using a transversely isotropic 1-D velocity model with linear velocity gradients (Table S3), based on the southeastern end of the SIST refraction profile (Bjarnason *et al.* 1993) and the northern part of the Katla refraction profile (Gudmundsson *et al.* 1994). Both profiles have similar velocity gradients and upper crustal thickness. We use a constant V_p/V_s ratio of 1.77, based on values derived from Wadati plots (Wadati 1933) of the manually picked event arrival times.

An initial catalogue of more than 20 000 microearthquakes during 5–20 2010 March was detected and located automatically using a coalescence microseismic mapping (CMM) technique (Drew *et al.* 2013; Fig. 2). The CMM method works by migrating continuously an onset function (based on a short-term average to long-term average ratio), calculated for each component at each station, into a subsurface search grid using forward-modelled travel times. Earthquake origin times and locations are obtained where there is a signal that coalesces in the search grid (Drew *et al.* 2013). The colour-coding in Fig. 2 denotes the strength of the coalescence signal for each earthquake. Higher coalescence values (blue dots) typically

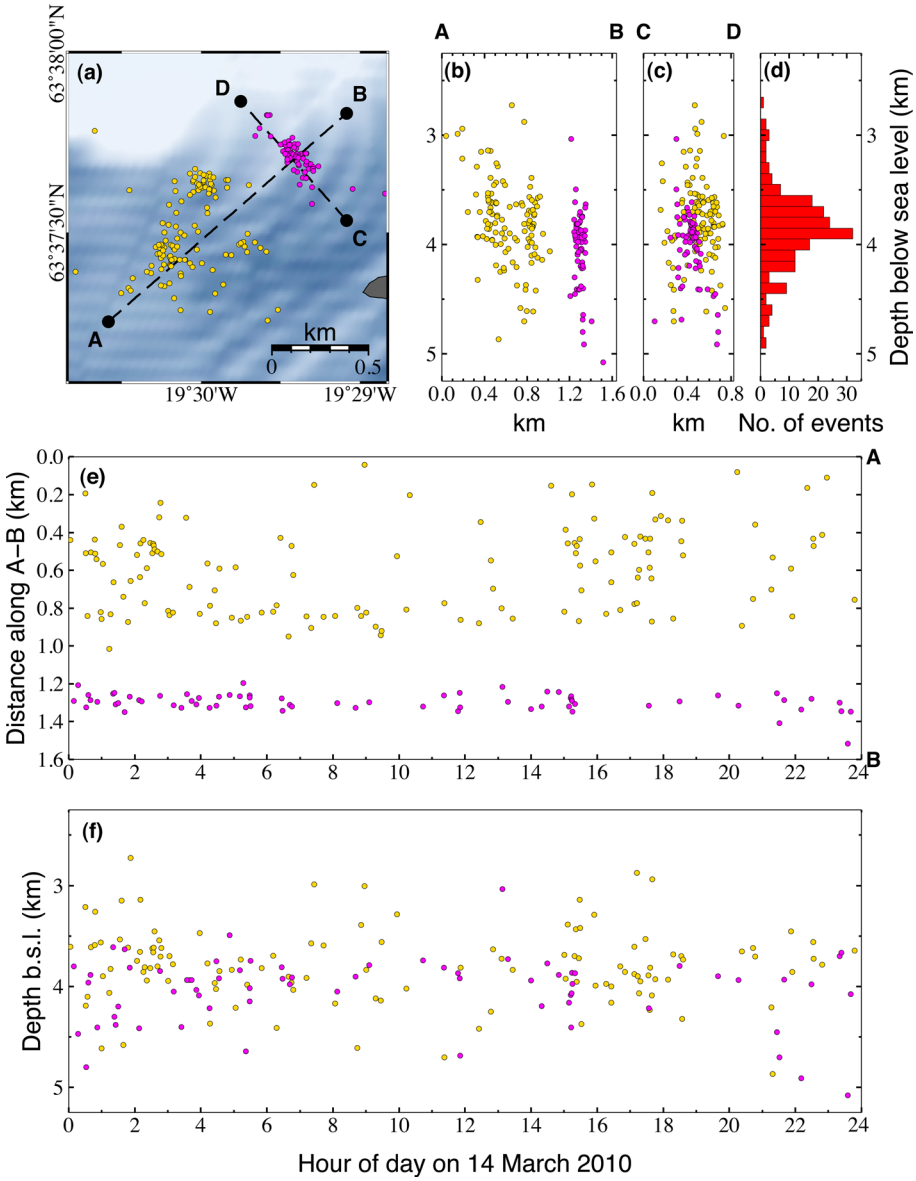

Figure 4. Spatial and temporal detail of a group of clusters in the southeast of the active region (for location see Fig. 3). All earthquakes shown occurred on 2010 March 14. (a) Map view of relocated hypocentres. (b) and (c) Cross sections of hypocentres projected onto lines A–B and C–D respectively. (d) Histogram of hypocentre depths. (e) Time-series of epicentres projected onto line A–B. (f) Time-series of hypocentre depths. Note there are three main clusters; events in the tightest cluster, to the northeast, are coloured purple throughout this figure so that they can be distinguished.

indicate events that have smaller location uncertainties, usually because they have larger magnitudes; events with lower coalescence values (red and yellow dots) have greater location uncertainties. The concentric pattern of epicentres in Fig. 2 is at least partly the result of greater location uncertainty and 'smearing' of epicentral locations for events with lower coalescence values, rather than necessarily reflecting the true earthquake distribution. The actual locus of seismic activity is probably restricted predominantly to the area covered by the blue (or blue and red) automatically located events with higher coalescence values.

A subset of 1095 earthquakes was selected from the automatic CMM catalogue for further analysis. These events were chosen on the basis of having either the strongest coalescence signals, or CMM hypocentre locations that already formed clear spatial clusters, especially in the east of the active region. *P*- and *S*-wave arrival times were picked manually and weighted for pick quality for each of the 1095 earthquakes. Hypoinverse (Klein 2002) was used to obtain single-event hypocentre locations with these manually refined arrival times (Fig. S1). Relative relocations were then calculated using the HypoDD double-difference algorithm (Waldhauser & Ellsworth 2000; Waldhauser 2001). A final catalogue of 1061 strongly linked, relatively relocated events was obtained in this way after 34 more weakly linked events were rejected (Fig. 3).

2.2 Hypocentre distribution

The spatial distribution of relatively relocated hypocentres forms a set of well-defined clusters under the east flank of the volcano, between the two eruption sites (Fig. 3; Animation 1). Five clear epicentral clusters lie in an approximately linear arrangement, running WNW–ESE, with 1.0–1.5 km between the centres of neighbouring clusters along the line. Other sets of clusters strike northeast from the clusters in this line, forming a second-order pattern of

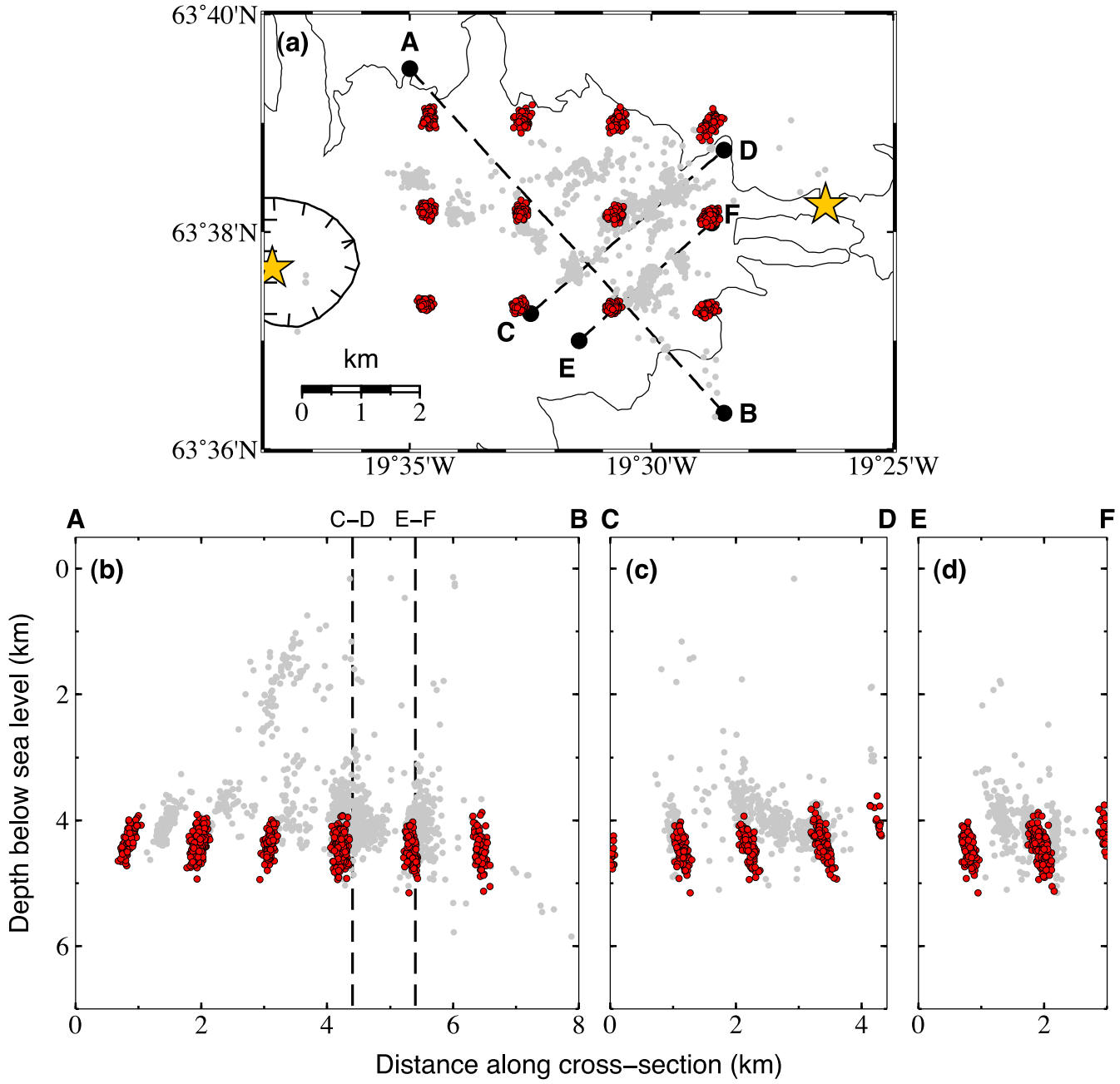

Figure 5. Effect of time-pick error on hypocentre locations. Grey circles show relatively relocated hypocentres for the real earthquakes from Fig. 3. Each cluster of red circles shows Hypoinverse locations for 100 sets of 'noisy' arrival times derived from the same parent set of exact arrival times. Random perturbations added to exact arrival times are normally distributed with a mean of zero and standard deviation of 0.02 s. Orange stars show eruption sites at Fimmvörðuháls (east) and Eyjafjallajökull summit (west). (a) Map view. (b–d) Cross-sections of hypocentres projected onto lines A–B, C–D and E–F respectively.

northeast–southwest alignment parallel to cross-section line C–D in Fig. 3.

Most hypocentres are located at 3.8 ± 0.5 km depth below sea level. Note that in this paper we show all depth distributions with one standard deviation about the mean, and depths with respect to sea level. The average surface elevation of the volcano above the seismicity discussed here is 1.25 km, so for subsurface depths the reader should add 1.25 km to the quoted depths below sea level. Each line of hypocentral clusters in this depth range comprises laterally distinct, separate clusters. The clusters have an apparent 1 km or more vertical extent, such that several clusters exhibit a subvertical pipe-like morphology (Figs 3 and 4). Shallower activity at <2 km occurred during the final 4 d prior to the initial eruption on 2010 March 20, with epicentres mostly in the central northern part of the active region (red and pink dots in Fig. 3). On the day of the eruption, very shallow seismicity (<1 km depth) extended close to the Fimmvörðuháls eruption site.

3 DYKES OR SILLS?

3.1 Vertically elongated seismic clusters

The pattern of multiple spatially separate clusters formed by the relocated hypocentres includes many that are apparently vertically

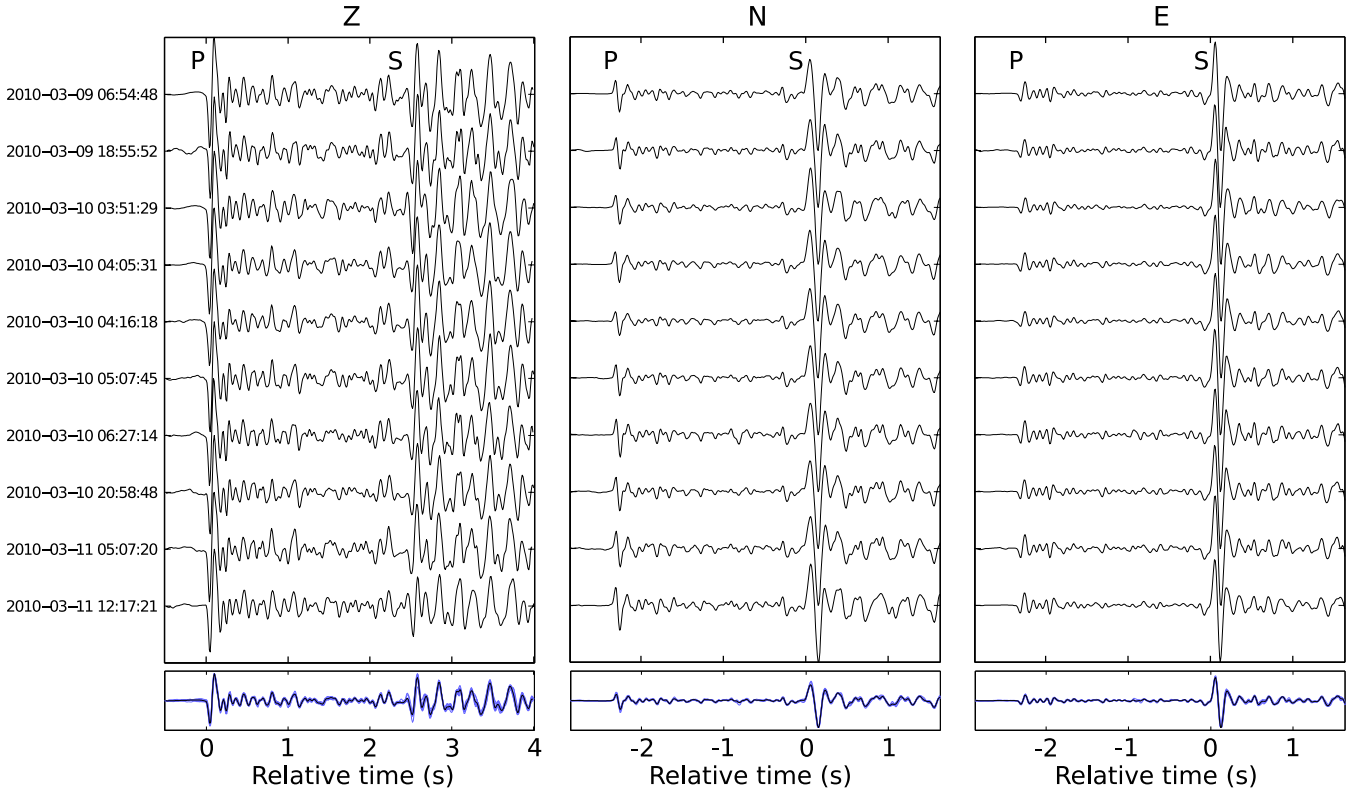

Figure 6. Similar waveforms for ten events in the westernmost cluster recorded at station ESK (see Fig. 2 for location). All three components for each event show no significant difference between events over a window containing both *P* and *S* arrivals. The Z (vertical) component traces are aligned on the *P* arrival; N and E (horizontal) components are aligned on the *S* arrival, but show the same time window of data as for the *Z* component for each event. Both *P* and *S* arrivals can be seen clearly on all three components. The bottom window for each component shows an overlay of waveforms for all 10 events (blue), with the average stack of all 10 events shown in black. All waveforms are bandpass-filtered between 2 and 25 Hz and are trace normalized.

elongated. The most striking example of this is the group of clusters in the southeast corner of the active region that are approximately vertical and parallel, with the vertical axis of each cluster separated by 300–500 m laterally from the next cluster (Figs 4b and c).

The vertically elongated shape of many of the hypocentral clusters may suggest that the pre-eruption magmatic intrusion occurred in a series of subvertical conduits, or dykes. If this were the case, such conduits might be separate, vertical pipes, fed by magma supply from below. Alternatively, the seismic clusters could delineate channels of relatively high (or low) vertical magma flux within planar, vertical dykes that contain the vertical seismic clusters. This interpretation would be consistent with 3-D field mapping of kimberlite dykes in South Africa that provides a well-constrained example of systematically varying dyke thickness (Kavanagh & Sparks 2011). In the kimberlite example, vertical 'channels' up to 1.9 m thick (i.e. normal to the plane of the dyke) are separated by much thinner sections of dyke that are only a few centimetres, or tens of centimetres, thick. In this scenario, seismicity may be generated by changes in flow rate in high-flux channels, or by re-fracturing of frozen and fused dyke walls in low-flux sections of the dyke when fresh melt is supplied (White *et al.* 2011).

Vertical conduits, separated laterally as are the seismic clusters, would require melt supply from below to feed into the bottom of each cluster. A sill that inflated just beneath the conduits might achieve this, with melt injecting sporadically upwards to form the vertical 'pipes' of seismicity. It may be that the base of the seismic clusters at ∼5 km depth represents the brittle-ductile transition in the crust beneath Eyjafjallajökull. A sharp cut-off in seismicity is observed to mark the brittle–ductile transition in the crust in other parts of Iceland. This is often at depths of 10 km or more, although it may be shallower within individual volcanic centres where the crust is hotter. For example, Soosalu *et al.* (2010) and Key *et al.* (2011a,b) report transition depths of 7–8 and 5–9 km, respectively, beneath Askja volcano in central Iceland.

However, whilst the morphology of the clusters might be taken to support an interpretation of seismogenic vertical magma conduits or dykes, several lines of evidence suggest that the vertical elongation of the seismic clusters is predominantly a location artefact, as we discuss next.

3.2 Hypocentral depth resolution

The configuration of the seismic network at Eyjafjallajökull is vulnerable to relatively large hypocentral depth uncertainties for earthquakes occurring at shallow depths (<5 km) under the flank of the volcano where most of the activity in question was observed (Tarasewicz *et al.* 2011). This vulnerability arises because the closest seismic stations are still ∼4 km away from the epicentres of the earthquakes (Fig. 2). Therefore, whilst azimuthal coverage of the earthquake sources is good (and epicentral locations are thus well constrained), the lack of stations directly overhead makes it difficult to resolve accurately the depths of shallow earthquakes.

The first indication that the vertical extent of the seismic clusters may be exaggerated is the depth distribution of earthquake hypocentres within clusters (Fig. 4d). The clusters shown in detail in Fig. 4 have hypocentral depth distributions that approximate normal distributions centred on the middle of each cluster. Such a

depth distribution is consistent with errors in travel times causing a spread about the true depth of 3.8 km rather than marking a real spread in hypocentral depths. In addition, there is no indication in the temporal distribution of earthquakes in each cluster that there is any consistent migration sequence up (or down) any of the clusters (Fig. 4f). If there were a clear progression of hypocentres moving up a cluster, that would support an interpretation either of a dyke propagating, or of a pulse of melt travelling up a pre-existing conduit (Taisne & Tait 2011; Massin *et al.* 2013). However, the lack of any such observation suggests that the clusters are not caused by the propagation of dyke tips through unfractured country rock, nor by pulses of melt travelling up pre-existing conduits.

Here, we have tested the effect of realistic arrival time uncertainties for the Eyjafjallajökull source–network geometry by adding random perturbations to exact modelled arrival times from synthetic sources under the flank of the volcano. A random travel-time perturbation from a normal distribution with a mean of zero was added to each synthetic arrival time. For each 'parent' set of exact arrival times, 100 different sets of perturbed 'noisy' synthetic arrival times were generated. Random perturbations were added independently to both *P* and *S* arrivals. The synthetic arrival picks were then inverted for the source location in the same way as were the real seismic data.

The result is to produce elongated clusters of hypocentre locations, centred on the true parent synthetic source location (red dots on Fig. 5). The synthetic clusters generated from a synthetic point source by adding random noise with a standard deviation of 0.02 s to the exact synthetic arrival times, strongly resemble the spatial distribution of hypocentres observed in the real seismic data (grey dots on Fig. 5). The extent of elongation of the clusters increases with the standard deviation of the random errors added to the arrival times from the parent source location. We consider a standard deviation of 0.02 s (as shown in Fig. 5) to be a realistic estimate of the actual uncertainty across all of our manual time picks.

Note that the horizontal spread of hypocentres due to random noise in each synthetic cluster is considerably less than is the vertical spread (Fig. 5). Therefore, the epicentres and horizontal separation of clusters are far more robust against noise in the arrival time picks than are the vertical locations (Figs 3a and 4a).

We conclude that the extent of vertical elongation of the real seismic clusters is likely to be exaggerated greatly as a result of small errors (of order 0.01–0.03 s) in the arrival time data. The synthetic noise tests suggest that each cluster of real earthquake hypocentres may be generated by a single, repeatedly active source in exactly the same location, analogous to the synthetic 'parent' source location for each synthetic cluster.

3.3 Cross-correlation of similar waveforms

Families of earthquakes with a high degree of similarity between waveforms have been observed within several of the clusters. This provides further evidence that the apparent vertical extent of the seismic clusters is exaggerated (in Figs 3 and 4). The best example of this is in the westernmost cluster of manually refined locations (Figs 6 and 7). Strong waveform correlation over a time window containing both the *P*- and *S*-wave arrivals reinforces the observation that the *P*-to-*S* time delay observed at each station does not vary significantly between events. For the *P*-to-*S* delay to be the same to within ~0.01 s, as is the case for several families of well-correlated waveforms (e.g. those in Fig. 6), the event separation must be less

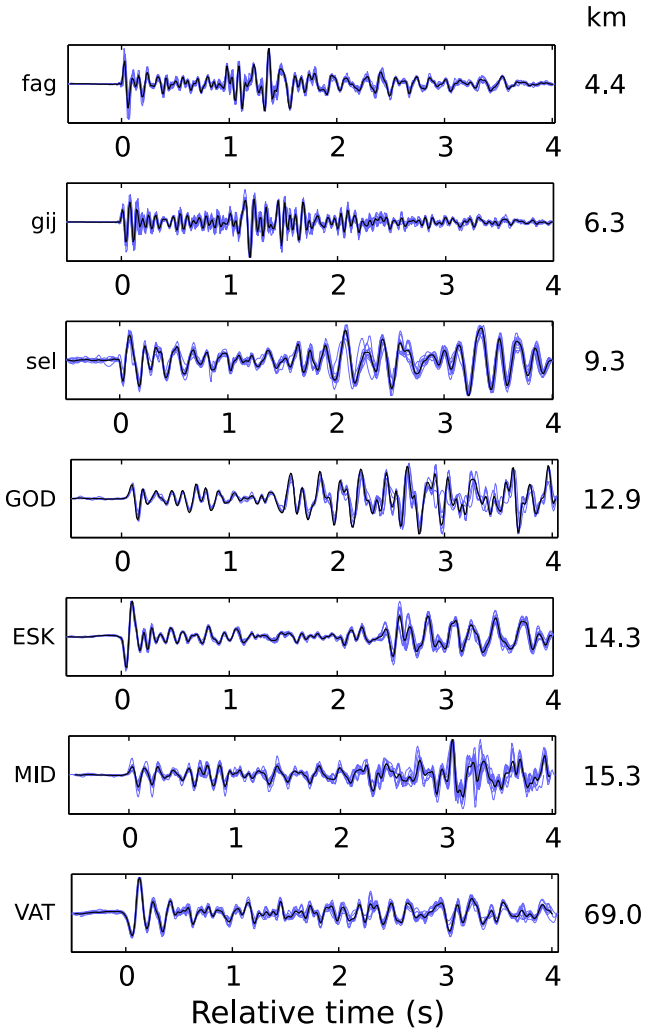

Figure 7. Overlay plots of vertical component traces for ten events in the westernmost cluster at the stations indicated (see Fig. 2 for locations of all seismometers shown except VAT, which lies at 64.1866°N, 18.9177°W). Individual event traces are plotted in blue; an average stack of all ten waveforms is shown in black for each station. All waveforms are bandpass-filtered between 2 and 25 Hz, aligned on the *P*-wave arrival and trace normalized. Distance of each station from the epicentre is indicated on right-hand side.

than ~65 m along the ray path (assuming $v_p = 5.0\,\mathrm{km\ s^{-1}}$ and $v_p/v_s = 1.77$ in the source region).

Relative relocation of events in this westernmost cluster using cross-correlated *P*- and *S*-wave arrival times with subsample time precision yields a much tighter hypocentral distribution than using only manual pick times (Fig. 8). The mean depth of events in this cluster is 3.84 ± 0.06 km when cross-correlation data are used (Fig. 8d). This cluster of 105 events comprises some of the largest-magnitude events, with the highest CMM coalescence signals in the data set, so are some of the best-constrained events.

In summary, the depth distribution of all the automatically CMM located events with signal-to-noise ratio (SNR) higher than 2.5, as shown by the red and blue symbols on Fig. 2 has a standard deviation of 1.46 km. This decreases to 0.95 km when only the best events with SNR higher than 3.5 are considered (blue symbols on Fig. 2). Manual picking of the arrival times from the best 1061 events followed by double-difference relocation further reduces the standard deviation by half to 0.5 km. Finally, for the best cluster of events in the centre of the seismometer array, refinement by

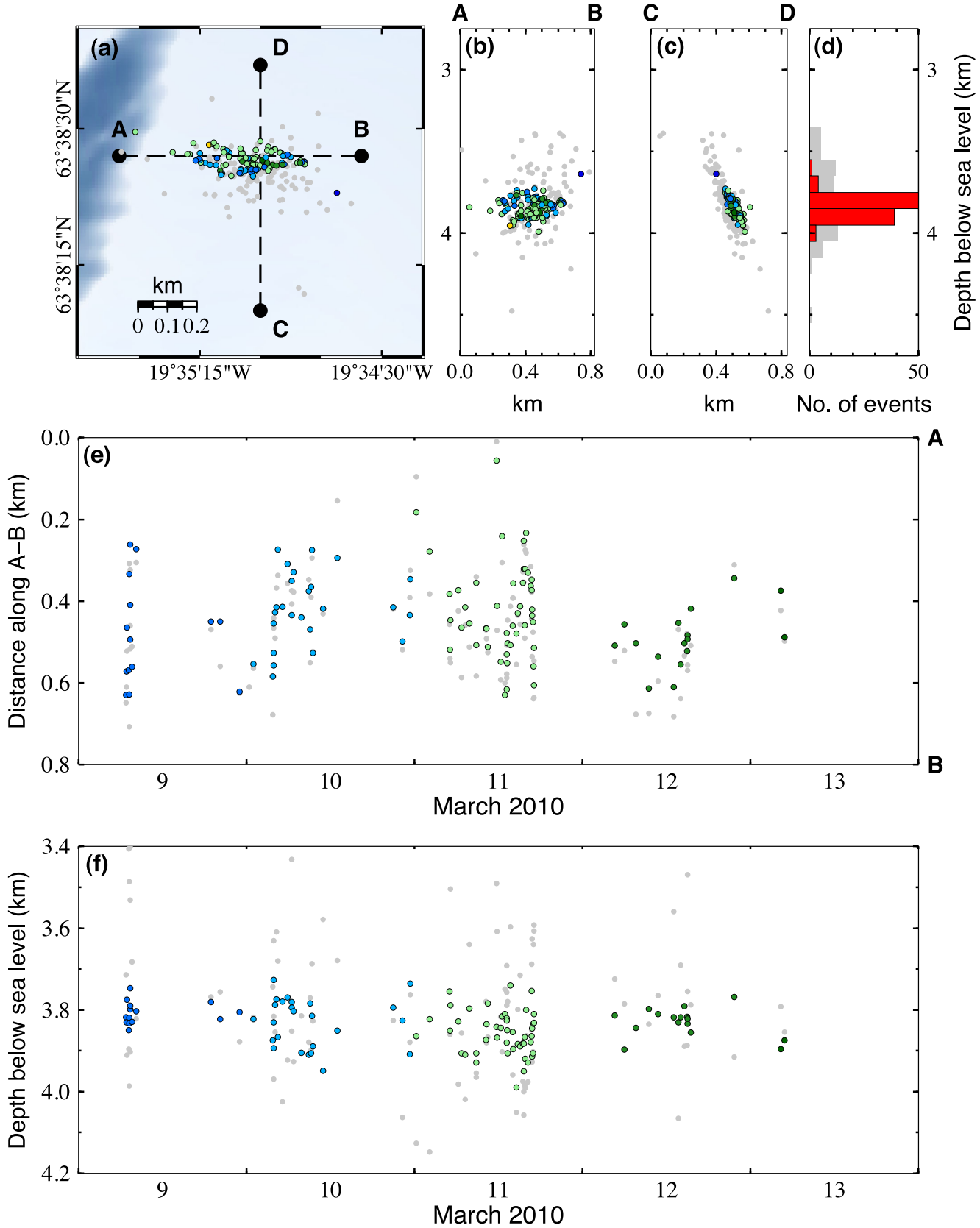

Figure 8. Spatial and temporal detail of westernmost cluster (for location see Fig. 3). (a) Map view of relocated event locations: coloured circles with solid outlines are hypocentres obtained using subsample cross-correlation arrival times for both *P* and S arrivals, and are colour-coded by date as in (e–f) and Fig. 3; grey circles are relative relocations for the same events excluding cross-correlation data, and are the same locations as plotted in Fig. 3. (b) and (c) Depth sections of hypocentres in (a) projected onto lines A–B and C–D, respectively. (d) Histogram of relocated hypocentre depths including (red) and excluding (grey) cross-correlation data. (e) Time-series of earthquake epicentres projected onto line A–B. (f) Time-series of hypocentre depths.

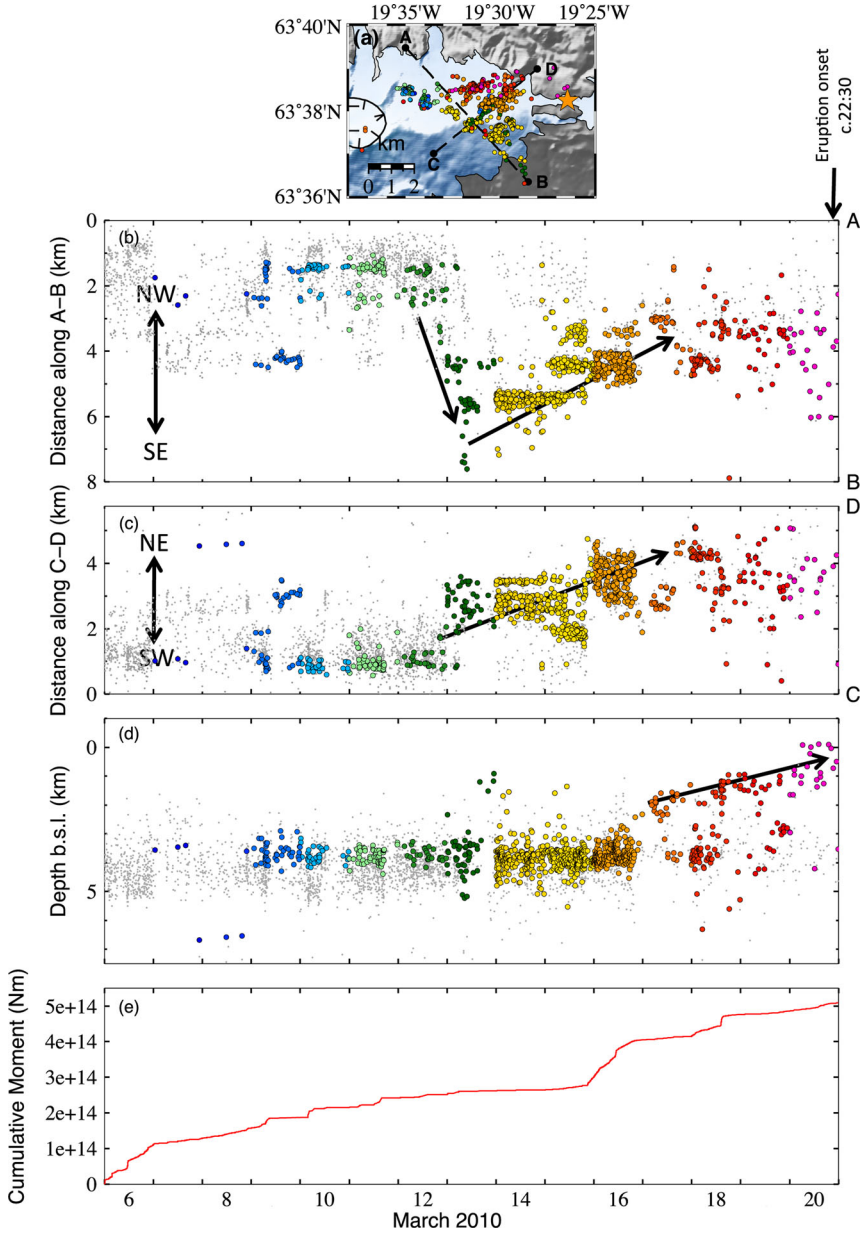

Figure 9. Time-series of pre-eruption, relatively relocated, hypocentre locations 2010 March 6–20. (a) Map view, colour-coded by date as in (b–d); orange star shows Fimmvörðuháls eruption site on 2010 March 20. (b) Epicentres from (a) projected onto line A–B; orientation of A–B chosen to highlight the separate clusters bounding the south edge of the active region, showing migration to the southeast on 2010 March 12–13 (arrow). Grey dots show CMM automatic locations, to show activity for which we have not manually refined the locations. (c) Epicentres projected onto C–D, showing progression of events to the northeast (arrow), particularly during 2010 March 15–16. (d) Hypocentre depths; note progressively shallower earthquakes occurred during 2010 March 17–20 (arrow). (e) Cumulative moment release during the period, calculated using magnitude estimates published by the Icelandic Meteorological Office (IMO); estimated earthquake magnitudes during this period range up to a maximum $M_L = 3.0$, with 29 earthquakes having $2.0 \leq M_L \leq 3.0$.

subsample cross-correlation of both *P* and *S* waves reduces the depth scatter by a further order of magnitude to 0.06 km. Although the coverage and SNR are not sufficiently good to achieve the same resolution from all the data, we consider it likely that most of the seismicity in the other clusters during March 5–20 actually occurred within a limited depth range and possibly all at the same 3.8 km depth as this cluster.

This is consistent with the seismicity being generated by lateral magma movement within a horizontally extensive intrusion complex at 3.8 km depth. The seismicity covers an area of 10 km^2, so if this marks the lateral extent of the sill complex, then the estimated ~0.05 km^3 of melt intrusion in the 3 months preceding the eruption (Sigmundsson *et al.* 2010), suggests that the sill inflated by an average of ~5 m.

3.4 Temporal pattern of activity

Initially, the seismic activity was concentrated just east of the summit caldera (Hjaltadóttir *et al.* 2012) and migrated eastward towards the Fimmvörðuháls eruption site during 2010 March 4–20 (Figs 3 and 9; Animation 2). There were notable shifts in the location of seismic activity, first to the southeast on March 12–13 (Fig. 9b), then subsequently to the northeast on March 15–16 (Fig. 9c). Seismic

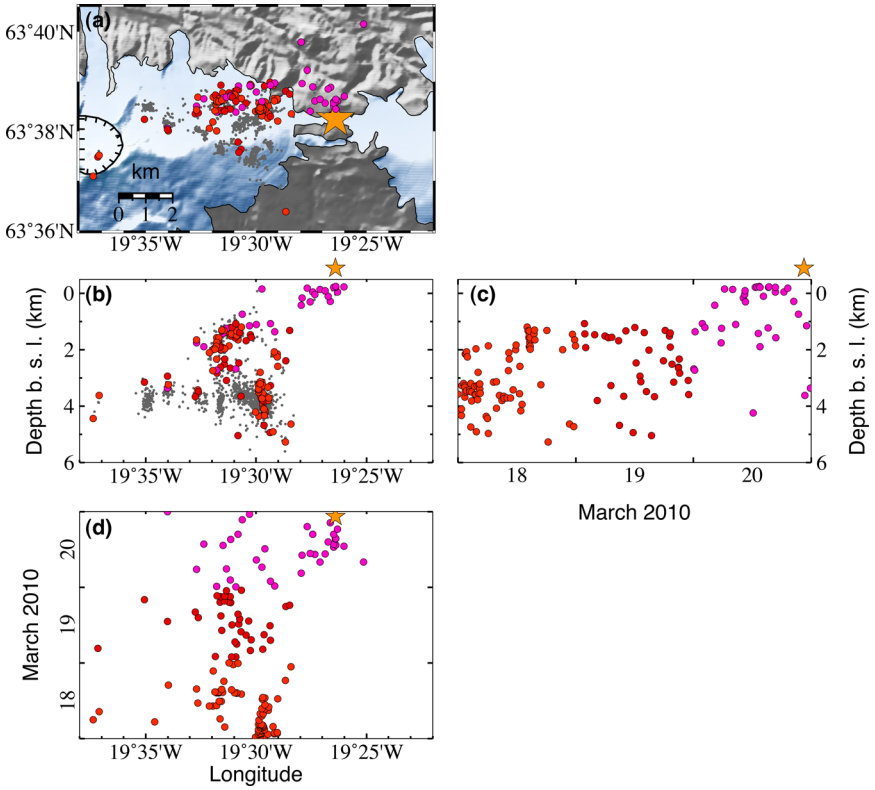

Figure 10. Seismicity recorded on 2010 March 17–20. (a) Map view of epicentres. (b) E–W depth section (no vertical exaggeration). (c) Time-series showing depth of hypocentres (aligned with (b)) during 2010 March 18–20; note shallowing progression over this period. (d) Time-series showing longitude of hypocentres (aligned with (a) and (b)) during 2010 March 18–20. Note progression to the east during 2010 March 20. Red/pink symbols are Hypoinverse single-event locations; note that some of the shallowest events shown here were rejected during the relative relocation process and are thus not plotted in earlier figures of relocated events. Dark grey dots show the data set of all relative relocations 2010 March 5–20. Orange stars show location [and onset time in (c–d)] of Fimmvörðuháls fissure eruption.

activity during March 5–16 was predominantly at ∼4 km depth. Shallower activity occurred at <2 km depth in the final 4 d prior to eruption (March 17–20), which we discuss in the following section.

During March 5–16, prior to the final few days of very shallow activity, many of the spatially separate clusters were active contemporaneously; there was not a simple, unidirectional migration of seismicity. Individual clusters were active persistently for several days, typically with episodic bursts of activity separated by relatively quiet periods lasting hours to days. These clusters of seismicity may have been generated in the overlying crust as it deformed to accommodate the magma intruding into lobes of the sill complex. However, we also find sets of microseismic events that are colocated to within the location uncertainty, and suggest that these may be occurring at pinch-points where melt is being forced laterally into separate lobes of the sill complex.

The temporal pattern of epicentre locations suggests that lateral melt migration within a horizontally extensive sill intrusion was the cause of the observed seismicity during March 5–16. The timing suggests that the intrusion was fed, at least initially, from the western end of the seismically active region, with melt propagating generally eastward towards the Fimmvörðuháls eruption site. The rapid increase in cumulative moment release (and also in the number of micro-earthquakes) that occurred on March 16 may represent a particularly large influx of melt into the sill complex at ∼4 km depth. It immediately preceded injection of the melt to much shallower levels which started on March 17, and eventually propagated upwards to eruption at the surface from the Fimmvörðuháls fissure.

4 SEISMIC EVIDENCE FOR A FEEDER DYKE TO THE SURFACE FISSURE

The intensity of seismic activity reduced markedly in the final 4 d before the Fimmvörðuháls fissure eruption (Fig. 9). There is no clear lateral migration of epicentres during March 17–19, during which time the shallow (<2 km) seismicity was concentrated in the central north part of the seismically active region (Fig. 10). However, on the morning of March 20, the day of the eruption, earthquake activity migrated 2–3 km further to the east than previously and the seismicity approached the eruption site, with many events located at <1 km depth. There is an overall shallowing trend in hypocentre depths over March 17–20 (Fig. 10c), although there are no obvious migration trends over shorter timescales of hours. It is possible that short-timescale migration trends do exist, but are masked by location uncertainties, which are likely to be greatest for the shallowest earthquakes at Eyjafjallajökull (Tarasewicz *et al.* 2011).

The seismicity is consistent with melt having progressed upward through the crust on March 17 where it may have ponded at ∼2 km depth approximately half-way between the two eruption sites. This shallower intrusion appears to have been active during the 4 d (March 17–20) prior to eruption. Finally, the seismicity suggests that a feeder dyke extended eastward to the Fimmvörðuháls eruption site, perhaps as late as the day of the eruption. The dyke may have been sourced from the intrusion at 3–4 km depth, or from the shallower intrusion at 1–2 km depth overlying the first. Seismicity continued at both crustal levels during March 18–19 before the

very shallow (<1 km) earthquakes occurred close to the eruption site on March 20.

5 SEISMOGENIC 'TRAPDOORS'

There are multiple sets of earthquakes during 2010 March 20 in which every earthquake in each set was located in the same place, perhaps even in exactly the same position, with events recurring on timescales of minutes to days. Not only are the hypocentres colocated to within the resolution of the network but also the waveforms are almost identical (Figs 6 and 7). This is the case on all three components over a time window encompassing both *P* and *S* arrivals (Fig. 6). This strong correlation of waveforms between events not only confirms that the earthquakes are colocated, but also indicates that the focal mechanisms for the earthquakes must be similar or identical.

For the westernmost cluster of 105 earthquakes (Fig. 8), only two individual *P*-wave first-motion polarity determinations out of 735 (0.3 per cent; Fig. 11) contradict the hypothesis that all events in the cluster except the first one have identical focal mechanisms. For this cluster, the best-fit double-couple fault-plane solutions have one shallow and one steeply dipping nodal plane (Fig. 12a). Fault planes from two other clusters elsewhere with repeating events show a similar result of one very shallow nodal plane and one subvertical nodal plane (Figs 12b and c). Although it is not possible from the fault-plane solution alone to determine which of the nodal planes is the fault plane, we suggest in our interpretation below that it is most likely to be the very shallowly dipping plane, which also happens to be the most tightly constrained plane. We can fit the impulsive waveforms by double-couple solutions, with no requirement for any volumetric component.

The similarity of both *P* and *S* waveforms and identical first-motion polarities across the network for sets of events within clusters require that the source mechanisms are similar within each cluster. The same sense of motion must occur on slip planes in approximately the same orientation that are approximately colocated. In some instances, these events occur several times within minutes of each other. The observations are consistent with many events in each cluster being generated on exactly the same fault plane, although subtle variations in the waveforms suggest that this is not necessarily the case for all events in each cluster.

The combination of colocated hypocentres (within error) and almost identical waveforms favours an interpretation that many of the seismic clusters are associated with persistently seismogenic 'trapdoors' that constrict lateral melt flow between segments of the sill complex (Fig. 13). These trapdoors may act as a form of pressure

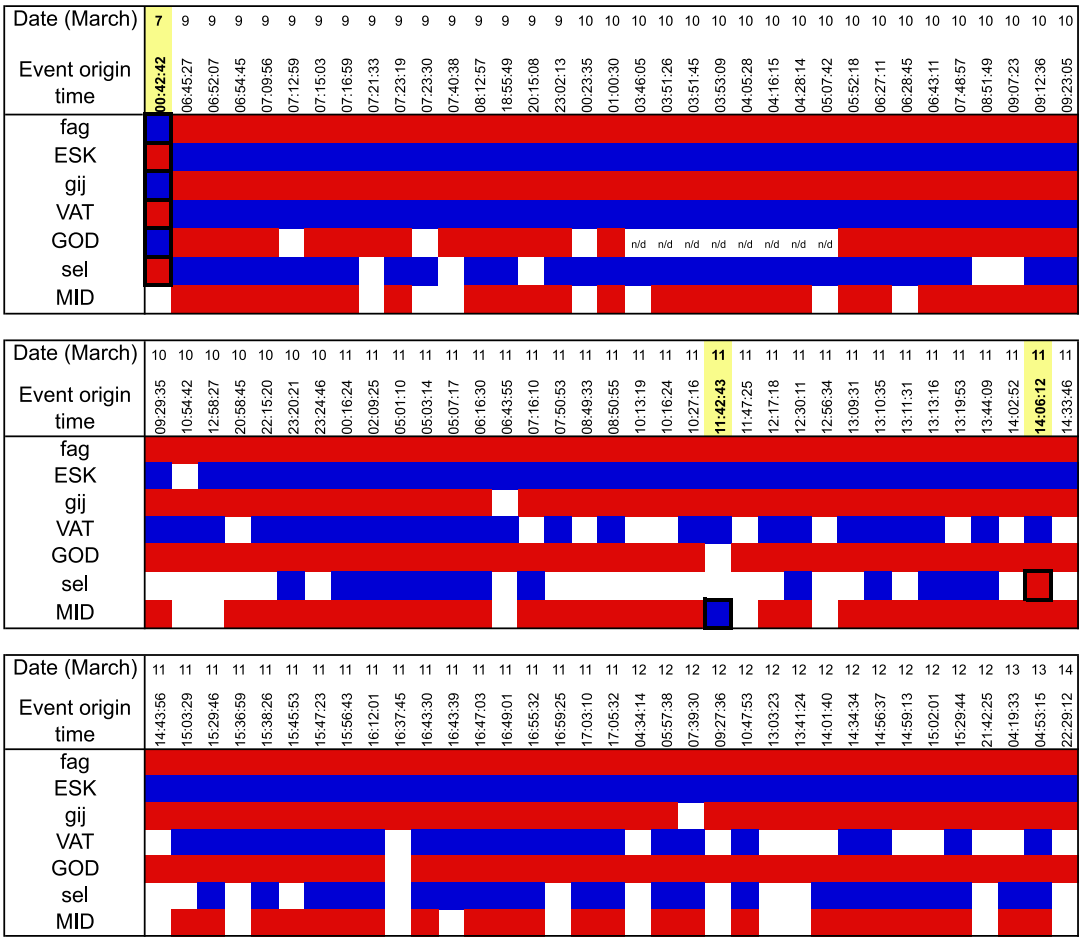

Figure 11. *P*-wave first-motion polarities for 105 events in the westernmost cluster. Red – compressional first motion; blue – dilatational first motion; blank – first-motion polarity unclear; n/d – no data from that station for those events (only affects GOD for 8 events). Event times highlighted show the three events that do not fit the polarity pattern of all other events: one is exactly opposite for all stations; the other two events have only one polarity that appears to be contrary to the pattern shared by the others. This suggests that all earthquakes except for the first have identical fault plane solutions; the first event has the exact opposite pattern of polarities, suggesting the opposite sense of motion on a similarly oriented plane.

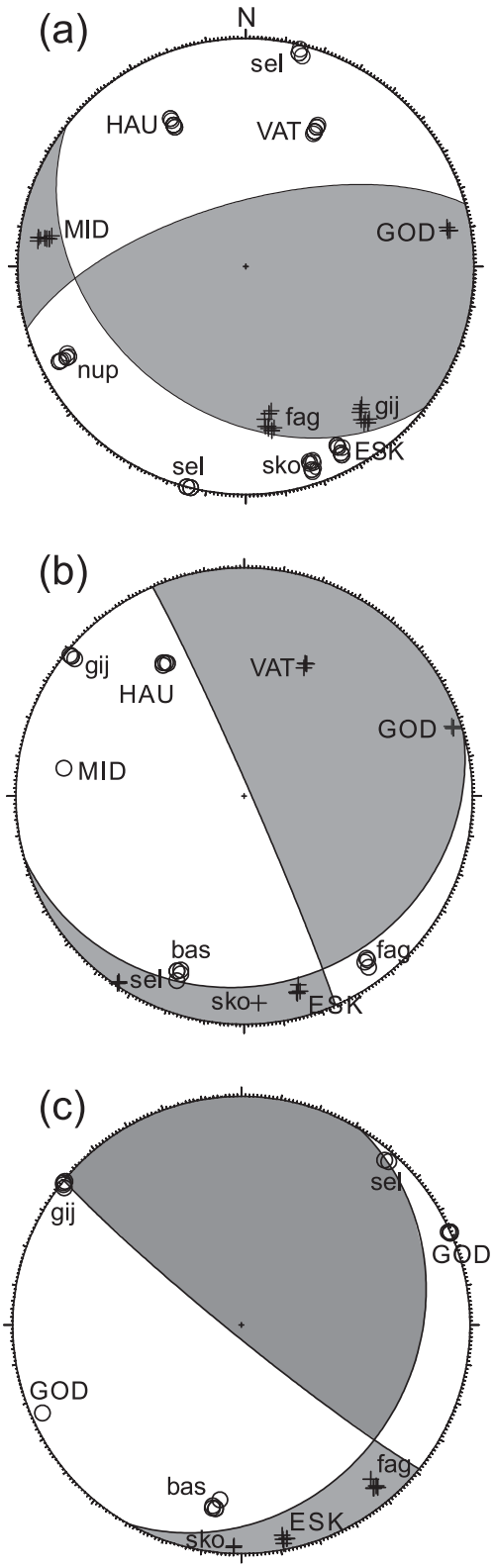

Figure 12. Double-couple composite fault-plane solution for multiple events from three different clusters (for locations see Fig. 3). (a) Cluster 1: calculated from events whose waveforms are shown in Fig. 7; Fig. 11 indicates that 104 of 105 events in the same cluster have the same pattern of *P*-wave first-motion polarities, suggesting a uniform focal mechanism solution. (b) Cluster 2. (c) Cluster 3. In each case we show the best-fit solution estimated using FPFIT (Reasenberg & Oppenheimer 1985), using a lower-hemisphere projection.

valve. If magma pressure builds up to one side of a constriction, it causes it to fracture and open an escape route for some magma. This would relieve pressure on the containing walls of the conduit such that the constriction reforms and the hot walls rapidly reseal. As magma pressure subsequently rebuilds, repeated fracturing may occur in the same location. Such a constriction could be a static 'trapdoor' where two conduit walls reseal or it could be a constriction inside the conduit between the country rock walls, such as a plug of solidified magma that moves only a short distance of a few millimetres or centimetres with each microearthquake. Between the seismic clusters there may be compartments of melt or aseismic conduits that allow flow without generating detectable seismicity. Note that we do not observe any very long period (VLP) events such as are often reported from conduits in the upper few hundred metres of the surface under other active volcanoes (e.g. Neuberg 2000; Ohminato 2006). The explanations for these VLP events require water vapour or gas bubbles within magma in vertical conduits: the events we report are at much greater pressures 5 km beneath the surface in thin (∼5 m thick) sills, and there is probably little free gas or vapour present at that depth.

Composite dykes, formed where earlier generations of melt have solidified and are refractured by the injection of later melts, are frequently reported in field studies (e.g. Irvine *et al.* 1998). However, it may not be necessary for melt to cool far below the solidus for fracturing to occur. Experiments measuring shear strength in cooling basalts show that a peak in shear strength is reached during the glass transition whilst still at high (∼0.7) homologous temperatures (White *et al.* 2012). This may mean that blockages can occur relatively easily in hot melt conduits, such that melt pressure can build up and refracture relatively hot rock, rather than simply flowing through aseismically.

A localised channel of high flow rate within a sill would also be consistent with field evidence from the Traigh Bhàn na Sgùrra sill on the Isle of Mull in Scotland. Holness and Humphreys (2003) report that two distinct sets of characteristics are evident in the sill from both the extent of the thermal metamorphic aureole in the country rock and the texture of dolerite in the sill. One has a thick metamorphic aureole and a coarse-grained contact with the country rock, suggesting prolonged flow through the sill lasting for several months, based on thermal arguments. Petrological and field evidence also indicates melting and assimilation of country rock into the sill in these sections. Other sections of the sill have chilled margins, only a thin metamorphic aureole and an increase in grain size towards the centre of the sill, all suggesting that there was only a single injection of melt into the country rock that chilled and solidified relatively quickly (Holness & Humphreys 2003). The first type that indicates prolonged flow is spatially arranged in channels within the sill, which may represent a fossil analogue for the distribution of flow regimes that could generate linear arrangements of seismicity such as the strings of clusters observed at Eyjafjallajökull.

Seismic imaging and field studies have found that some magmatic intrusions form as a series of subhorizontal lobes, which may overlap and interconnect as they inflate (Schofield *et al.* 2012). The host rock between inflating lobes of an intrusion may also be possible sites of seismogenic deformation recurring in fixed locations, with aseismic magma lobes separating seismic clusters.

A small number of earthquakes exhibit 'mirror image' waveforms, suggesting the opposite sense of motion to the great majority of earthquakes in the cluster, but on the same, or similar, orientation of failure plane. The first event in the sequence of 105 earthquakes in the westernmost cluster is one example of this (Fig. 14). 'Flipped' waveforms have also been observed in a set of similar waveforms

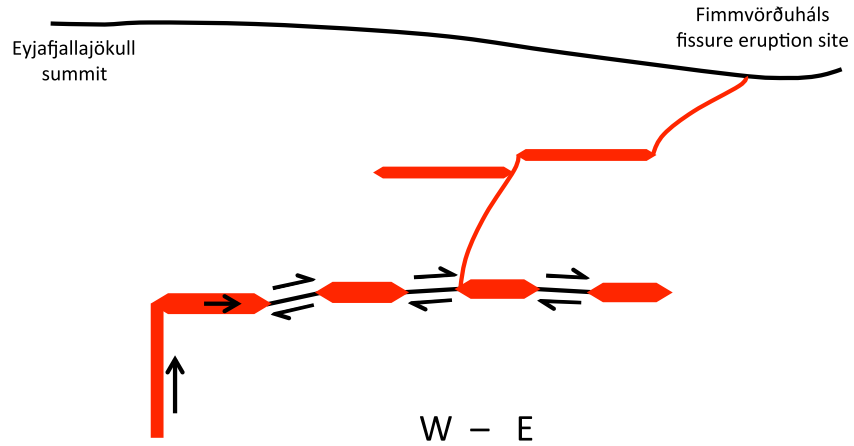

Figure 13. Cartoon schematic E–W cross-section (not to scale) showing compartments or lobes of an intrusion fed by magma influx from the left (west) and linked by seismogenic 'trapdoors'. Shear failure on fault planes such as those indicated may result from pulses of melt passing from one compartment to the next, generating the observed seismic clusters in spatially fixed locations. The shallower intrusion and dyke suggested by seismicity at <2 km during the 4 d prior to the eruption are also shown schematically.

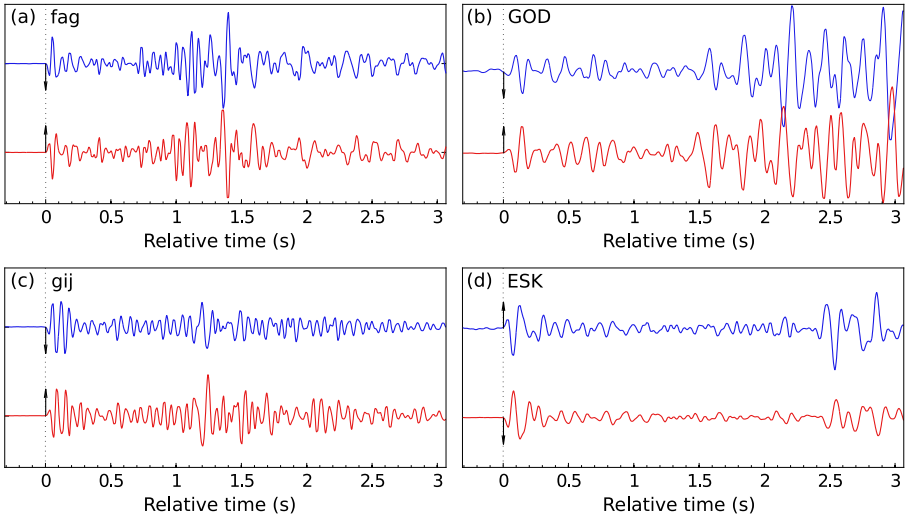

Figure 14. 'Mirror image' waveforms. Traces are vertical-component velocity, aligned on *P* arrivals and bandpass filtered at 2–25 Hz, recorded at the stations indicated (see Fig. 2 for locations). Blue traces are for the first event in the westernmost cluster, at 00:42:42 on 2010 March 7; red traces are for the second event, at 06:45:27 on 2010 March 9 (see also Fig. 10). Arrows show direction of *P*-wave first motion.

associated with seismicity in an inclined mid-crustal dyke at Upptyppingar in the Northern Volcanic Zone of Iceland (White *et al.* 2011). The failure planes are precisely parallel to the macroscopic dip of the dyke, so are either within the dyke or in the immediately adjacent country rock. These faults are attributed to magma shunting solidified plugs along and generating seismicity between the plug and the dyke walls. In this scenario, as the plug moves up the dyke, opposite senses of slip are generated on either side of the plug, on parallel failure planes. This is a possible mechanism to explain sets of approximately colocated earthquakes at Eyjafjallajökull with both similar and 'flipped' waveforms. Alternatively, pressurisation and depressurisation of magma could cause persistent slip on a weak plane between pockets or compartments of magma.

A similar behaviour of repeated, almost identical, seismic multiplets at fixed locations was observed during the 1983 propagation of a dyke in Kilauea (Rubin & Gillard 1998). These were termed 'hotspots' and, like the multiplets we report here, they sometimes exhibited completely inverted waveforms, which may represent a reversal of slip on the same fault or on either side of the dyke due to changes in pressurisation of the magma (e.g. see fig. 10 of Rubin & Gillard 1998).

5 CONCLUSIONS

We have manually refined arrival time picks for over 1000 earthquakes recorded during 2010 March 5–20, immediately prior to the eruption of Fimmvörðuháls on the eastern margin of Eyjafjallajökull volcano in Iceland. Relative relocations of these events lie predominantly in a series of laterally distinct clusters at ∼4 km depth under the east flank of the volcano between the two subsequent eruption sites. There is also seismic evidence for intrusion of magma at ∼2 km depth in the final 4 d before eruption and for a feeder dyke extending from the region of precursory active seismicity towards the first eruption site at Fimmvörðuháls.

Synthetic tests demonstrate that the network geometry is susceptible to vertical location uncertainty. The observed orientation and morphology of clusters of hypocentres can be replicated by adding

very small amounts of random noise to synthetic arrival time data for a single synthetic source location at the centre of each cluster. Furthermore, many clusters contain sets of events with almost identical waveforms, with no significant shift in *P*-to-*S* delay times between events. Cross-correlation of similar waveforms in a cluster results in a reduction of the depth uncertainty by an order of magnitude.

Waveform similarity observed at multiple stations is striking for sets of up to tens of events in some clusters. Where this is the case, all such events in a set may be generated in a single, static location that is repeatedly active, with the same orientation and sense of failure.

We interpret the clusters of repeating seismic sources in fixed locations as possible seismogenic 'trapdoors' within an inflating sill (or between lobes or compartments of a more complex intrusion) that occur at constrictions to melt flow within the intrusion that may act as pressure valves. The more widely spread pattern of epicentres in which these colocated 'trapdoor' events lie may be caused by faulting in the country rock as it deforms to accommodate the influx of melt into the inflating sill.

ACKNOWLEDGEMENTS

Seismic data were acquired using instruments from the LOKI instrument pool (owned jointly by the Icelandic Meteorological Office, the Institute of Earth Sciences, University of Iceland and Iceland GeoSurvey), supplemented by data from the Icelandic Meteorological Office's permanent monitoring network. We thank M. Hensch, S. Steinthórsson, Th. Jónsson, Ó. Gudmundsson, B. Ófeigsson, the helicopter crew of the Icelandic Coast Guard and others who assisted with Eyjafjallajökull fieldwork. We thank Arthur Jolly for comments which improved the paper. J. Drew provided the CMM code. R. Paren assisted with data reduction. Cross-correlation and waveform figures used the GISMO suite of MATLAB codes (Reyes & West 2011). Other figures were made using Generic Mapping Tools (GMT; Wessel & Smith 1998). JT was funded by the UK's National Environment Research Council (NERC). Department of Earth Sciences, Cambridge, contribution ESC2966.

REFERENCES

Bjarnason, I.T., Menke, W., Flóvenz, O.G. & Caress, D., 1993. Tomographic image of the Mid-Atlantic plate boundary in Southwestern Iceland, *J. geophys. Res.,* **98,** 6607–6622.

Dahm, T. & Brandsdóttir, B., 1997. Moment tensors of microearthquakes from the Eyjafjallajökull volcano in south Iceland, *Geophys. J. Int.,* **130,** 183–192.

Drew, J., White, R.S., Tilmann, F. & Tarasewicz, J., 2013. Coalescence Microseismic Mapping, *Geophys. J. Int.,* **195,** 1773–1785.

Edwards, B. *et al.*, 2012. Interactions between snow/firn/ice and lava/tephra during the 2010 Fimmvörðuháls eruption, south-central Iceland, *J. geophys. Res.,* **117,** B04302, doi:10.1029/2011JB008985.

Einarsson, P., 1991. Earthquakes and present-day tectonism in Iceland, *Tectonophysics,* **189,** 261–279.

Einarsson, P., 2010. Mapping of Holocene surface ruptures in the South Iceland Seismic Zone, *Jökull,* **60,** 121–138.

Einarsson, P. & Brandsdóttir, B., 2000. Earthquakes in the Mýrdalsjökull area, Iceland, 1978–1985: Seasonal correlation and connection with volcanoes, *Jökull,* **49,** 59–73.

Einarsson, P. & Sæmundsson, K., 1987. Earthquake epicentres 1982–1985 and volcanic systems in Iceland, in *Í hlutarins eðli*, Festschrift for Thorbjörn Sigurgeirsson, ed. Sigfússon, Th., Menningarsjóður, Reykjavík (map).

Gudmundsson, O., Brandsdóttir, B., Menke, W. & Sigvaldason, G.E., 1994. The crustal magma chamber of the Katla volcano in south Iceland revealed by 2-D seismic undershooting, *Geophys. J. Int.,* **119,** 277–296.

Gudmundsson, M.T. *et al.*, 2012a. Ash generation and distribution from the April-May 2010 eruption of Eyjafjallajökull, Iceland, *Sci. Rep.,* **2,** 572, doi:10.1038/srep00572.

Gudmundsson, M.T. *et al.*, 2012b. Scientific aspects: discussion and analysis, in *The 2010 Eyjafjallajökull Eruption, Iceland*, Chapter 5.1, pp. 101–114, ed. Thorkelsson, B., Report to the International Civil Aviation Organization (ICAO), by the Icelandic Meteorological Office, Institute of Earth Sciences, University of Iceland and the Department of Civil Protection and Emergency Management of the National Commissioner of the Icelandic Police, Reykjavík.

Hjaltadóttir, S., Vogfjörð, K.S. & Slunga, R., 2009. Seismic signs of magma pathways through the crust in the Eyjafjallajökull volcano, South Iceland, *Icelandic Meteorological Office Report*, VI 2009–013, Reykjavík.

Hjaltadóttir, S. *et al.*, 2012. 2010 pre-eruption phase, in *The 2010 Eyjafjallajökull Eruption, Iceland*, Chapter 4.2, pp. 49–54, ed. Thorkelsson, B., Report to the International Civil Aviation Organization (ICAO), by the Icelandic Meteorological Office, Institute of Earth Sciences, University of Iceland and the Department of Civil Protection and Emergency Management of the National Commissioner of the Icelandic Police, Reykjavík.

Holness, M.B. & Humphreys, M.C.S., 2003. The Traigh Bhàn na Sgùrra Sill, Isle of mull: flow localization in a major magma conduit, *J. Petrol.,* **44**(11), 1961–1976.

Höskuldsson, Á. *et al.,* 2012. Flank eruption at Fimmvörðuháls, in *The 2010 Eyjafjallajökull Eruption, Iceland*, Chapter 4.3, pp. 54–65, ed. Thorkelsson, B., Report to the International Civil Aviation Organization (ICAO), by the Icelandic Meteorological Office, Institute of Earth Sciences, University of Iceland and the Department of Civil Protection and Emergency Management of the National Commissioner of the Icelandic Police, Reykjavík.

Hreinsdóttir, S. *et al.*, 2012. The 2010 Eyjafjallajökull and 2011 Grímsvötn eruptions: Insights from GPS geodesy, *Geophys. Res. Abstr.,* **14,** EGU2012-13577-1.

Irvine, T.N., Andersen, J.C.Ø. & Brooks, C.K., 1998. Included blocks (and blocks within blocks) in the Skaergaard intrusion: Geologic relations and the origins of rhythmic modally graded layers, *GSA Bull.,* **110,** 1398–1447.

Jakobsdóttir, S.S., 2008. Seismicity in Iceland: 1994–2007, *Jökull,* **58,** 75–100.

Jóhannesson, H. & Sæmundsson, K., 1998. Geological map of Iceland, bedrock geology, scale 1:500,000, Icelandic Inst. of Natl. Hist. and Icelandic Geod. Surv., Reykjavík.

Kavanagh, J.L. & Sparks, R.S.J., 2011. Insights of dyke emplacement mechanics from detailed 3D dyke thickness datasets, *J. Geol. Soc. Lond.,* **168,** 965–978.

Keiding, J.K. & Sigmarsson, O., 2012. Geothermobarometry of the 2010 Eyjafjallajökull eruption: new constraints on Icelandic magma plumbing systems, *J. geophys. Res.,* **117,** B00C09, doi:10.1029/2011JB008829.

Key, J., White, R.S., Soosalu, H.E. & Jakobsdóttir, S.S., 2011a. Multiple melt injection along a spreading segment at Askja, Iceland, *Geophys. Res. Lett.,* **38,** L05301, doi:10.1029/2010GL046264.

Key, J., White, R.S., Soosalu, H.E. & Jakobsdóttir, S.S., 2011b. Correction to "Multiple melt injection along a spreading segment at Askja, Iceland," *Geophys. Res. Lett.,* **38,** L10308, doi:10.1029/2011GL047491.

Klein, F.W., 2002. User's guide to HYPOINVERSE-2000, a FORTRAN program to solve for earthquake locations and magnitudes, U.S. Geol. Surv. Open File Rep., 02–171, 123 pp.

Larsen, G., Pedersen, R. & Ilyinskaya, E., 2012. The Eyjafjallajökull volcano, in *The 2010 Eyjafjallajökull Eruption, Iceland*, Chapter 4.1, pp. 45–48, ed. Thorkelsson, B., Report to the International Civil Aviation Organization (ICAO), by the Icelandic Meteorological Office, Institute of Earth Sciences, University of Iceland and the Department of Civil Protection and Emergency Management of the National Commissioner of the Icelandic Police, Reykjavík.

Magnússon, E., Gudmundsson, M.T., Roberts, M.J., Sigurðsson, G., Höskuldsson, F. & Oddsson, B., 2012. Ice-volcano interactions during the 2010 Eyjafjallajökull eruption, as revealed by airborne imaging radar, *J. geophys. Res.,* **117,** B07405, doi:10.1029/2012JB009250.

Massin, F., Farrell, J. & Smith, R.B., 2013. Repeating earthquakes in the Yellowstone volcanic field: implications for rupture dynamics, ground deformation, and migration in earthquake swarms, *J. Volc. Geotherm. Res.,* **257,** 159–173.

Neuberg, J., 2000. Characteristics and causes of shallow seismicity in andesite volcanoes, *Phil. Trans. R. Soc. Lond., A*, **358,** 1533–1546.

Ohminato, T., 2006. Characteristics and source modeling of broadband seismic signals associated with the hydrothermal system at Satsuma–Iwojima volcano, Japan, *J. Volc. Geotherm. Res.,* **158,** 467–490.

Óskarsson, B.V., 2009. The Skerin ridge on Eyjafjallajökull, south Iceland: Morphology and magma-ice interaction in an ice-confined silicic fissure eruption, *MS thesis*, Fac. of Earth Sci., Univ. of Iceland, Reykjavík.

Pedersen, R. & Sigmundsson, F., 2004. InSAR based sill model links spatially offset areas of deformation and seismicity for the 1994 unrest episode at Eyjafjallajökull volcano, Iceland, *Geophys. Res. Lett.,* **31,** L14610, doi:10.1029/2004GL020368.

Pedersen, R. & Sigmundsson, F., 2006. Temporal development of the 1999 intrusive episode in the Eyjafjallajökull volcano, Iceland, derived from InSAR images, *Bull. Volcanol.,* **68,** 377–393.

Reasenberg, P. & Oppenheimer, D., 1985. FPFIT, FPPLOT and FPPAGE: Fortran computer programs for calculating and displaying earthquake fault-plane solutions, USGS Open-File Report No. 85–739.

Reyes, C.G. & West, M.E., 2011. The waveform suite; a robust platform for manipulating waveforms in MATLAB, *Seismol. Res. Lett.,* **82**(1), 104–110.

Rubin, A.M. & Gillard, D., 1998. A reinterpretation of seismicity associated with the January 1983 dike intrusion at Kilauea Volcano, Hawaii, *J. geophys. Res.,* **103,** 10 003–10 015.

Schofield, N., Heaton, L., Holford, S.P., Archer, S.G., Jackson, C.A.-L. & Jolley, D.W., 2012. Seismic imaging of 'broken bridges': linking seismic to outcrop-scale investigations of intrusive magma lobes, *J. Geol. Soc. Lond.,* **169,** 421–426.

Sigmundsson, F. *et al.*, 2010. Intrusion triggering of the 2010 Eyjafjallajökull explosive eruption, *Nature,* **468,** 426–430.

Soosalu, H., Key, J., White, R.S., Knox, C., Einarsson, P. & Jakobsdóttir, S.S., 2010. Lower-crustal earthquakes caused by magma movement beneath Askja volcano on the north Iceland rift, *Bull. Volcanol.,* **72**(1), 55–62.

Sturkell, E., Sigmundsson, F. & Einarsson, P., 2003. Recent unrest and magma movements at Eyjafjallajökull and Katla volcanoes, Iceland, *J. geophys. Res.,* **108**(B8), 2369, doi:10.1029/2001JB000917.

Taisne, B. & Tait, S., 2011. Effect of solidification on a propagating dike, *J. geophys. Res.,* **116,** B01206, doi:10.1029/ 2009JB007058.

Tarasewicz, J., White, R.S., Brandsdóttir, B. & Thorbjarnardóttir, B., 2011. Location accuracy of earthquake hypocentres beneath Eyjafjallajökull, Iceland, prior to the 2010 eruptions, *Jökull,* **61,** 33–50.

Tarasewicz, J., Brandsdóttir, B., White, R.S., Hensch, M. & Thorbjarnardóttir, B., 2012a. Using microearthquakes to track repeated magma intrusions beneath the Eyjafjallajökull stratovolcano, Iceland, *J. geophys. Res.,* **117,** B00C06, doi:10.1029/ 2011JB008751.

Tarasewicz, J., White, R.S., Woods, A.W., Brandsdóttir, B. & Gudmundsson, M.T., 2012b. Magma mobilization by downward-propagating decompression of the Eyjafjallajökull volcanic plumbing system, *Geophys. Res. Lett.,* **39,** L19309, doi:10.1029/2012GL053518.

Wadati, K., 1933. On the travel time of earthquake waves, Part II, *Geophys. Mag.,* **7,** 101–111.

Waldhauser, F., 2001. HypoDD: A program to compute double-difference hypocenter locations, USGS Open File Report, 01–113.

Waldhauser, F. & Ellsworth, W.L., 2000. A double-difference earthquake location algorithm: Method and application to the Northern Hayward Fault, California, *Bull. seism. Soc. Am.,* **90,** 1353–1368.

Wessel, P. & Smith, W.H.F., 1998. New, improved version of the Generic Mapping Tools released, *EOS, Trans. Am. geophys. Un.,* **79**(47), 579, doi:10.1029/98EO00426.

White, R.S., Drew, J., Martens, H.R., Key, A.J., Soosalu, H. & Jakobsdóttir, S.S., 2011. Dynamics of dyke intrusion in the mid-crust of Iceland, *Earth planet. Sci. Lett.,* **304,** 300–312.

White, R.S., Redfern, S.A.T. & Chien, S.-Y., 2012. Episodicity of seismicity accompanying melt intrusion into the crust, *Geophys. Res. Lett.,* **39,** L08306, doi:10.1029/2012GL051392.

SUPPORTING INFORMATION

Additional Supporting Information may be found in the online version of this article:

Figure S1. Single-event hypocentre locations obtained using Hypoinverse (Klein 2002). (a) Map view. (b) E–W cross-section. Hypoinverse hypocentres are plotted in red for the 1095 events with manually picked *P*- and *S*-wave arrival times. Grey dots show CMM automatic locations for events with SNR > 2.5.

Animation 1: 3-D rotating view of relatively relocated pre-eruption hypocentres. The same HypoDD hypocentres are shown as in Fig. 3, for 1061 events with manually picked arrival times, colour-coded by date. The black arrow points north; the red triangle shows location of Fimmvörðuháls eruption site on 2010 March 20. The animation begins in map view (as in Fig. 3a) then rotates to a viewpoint of 10° above horizontal, after which it rotates 360° about a vertical axis.

Animation 2: Time-series animation showing sequence of automatic (CMM) epicentres prior to the eruption (2010 March 5–20). Each frame of the animation shows 1 d of activity detected using CMM for events with SNR >2.0 and with vertical and horizontal CMM location uncertainties of <2.5 km and <1.0 km, respectively (see also Fig. 2). Orange star shows Fimmvörðuháls eruption site. Triangles show seismometer locations.

Table S1. Catalogue of earthquake locations associated with the 2010 Eyjafjallajökull eruption. Hypocentre locations stated are relatively relocated using HypoDD (Waldhauser 2001) with manual *P*- and *S*-wave arrival time picks and the velocity model in Table 3.

Table S2. Catalogue of earthquake locations for the cluster shown in Fig. 8, relatively relocated using HypoDD (Waldhauser 2001) with both manual and cross-correlated arrival time picks for both *P* and *S* waves. The velocity model in Table S3 was used for the relocations.

Table S3. Linear-gradient, one-dimensional, velocity model used to locate earthquakes at Eyjafjallajökull (http://gji.oxfordjournals.org/lookup/suppl/doi:10.1093/gji/ggt169/-/DC1)

Please note: Oxford University Press is not responsible for the content or functionality of any supporting materials supplied by the authors. Any queries (other than missing material) should be directed to the corresponding author for the article.